Dalton Transactions

RSC Publishing

PAPER

View Article Online
View Journal | View Issue

Cite this: *Dalton Trans.*, 2013, **42**, 2822

Novel MoO_2/carbon hierarchical nano/microcomposites: synthesis, characterization, solid state transformations and thiophene HDS activity†

Carlos Avendaño,[a] Alexander Briceño,*[a] Franklin J. Méndez,[a] Joaquín L. Brito,[a] Gema González,[b] Edgar Cañizales,[c] Reinaldo Atencio[d] and Philippe Dieudonné[e]

Novel MoO_2/C nano/microcomposites were prepared *via* a bottom-up approach by hydrothermal carbonization of a solution of glucose as a carbon precursor in the presence of polyoxometalates (POMs: phosphomolybdic acid $[H_3PMo_{12}O_{40}]$ and ammonium heptamolybdate tetrahydrate $[(NH_4)_6Mo_7O_{24}]\cdot 4H_2O$). The structural characterization by FT-IR, XRPD, SEM and TEM analyses revealed the controlled formation of hierarchical MoO_2/C composites with different morphologies: strawberry-like, based on carbon microspheres decorated with MoO_2 nanoparticles; MoO_2/C core–shell composites; and irregular aggregates in combination with ring-like microstructures bearing amorphous Mo species. These composites can be fine-tuned by varying reaction time, glucose/POM ratio and type of POM precursor. Subsequent transformations in the solid state through calcinations of MoO_2/C core–shell composites in air lead to hollow nanostructured molybdenum trioxide microspheres together with nanorods and plate microcrystals or cauliflower-like composites (MoO_2/C). In addition, the MoO_2/C composite undergoes a morphology evolution to urchin-like composites when it is calcined under nitrogen atmosphere (MoO_2/C–N_2). The MoO_2/C strawberry-like and MoO_2/C–N_2 composites were transformed into Mo carbide and nitride supported on carbon microspheres (Mo_2C/C, MoN/C, and MoN/C–N_2). These phases were tested as precursors in thiophene hydrodesulphurization (HDS) at 400 °C, observing the following trend in relation to the thiophene steady-state conversion: MoN/C–N_2 > MoN/C > Mo_2C/C > MoO_2/C–N_2 > MoO_2/C. According to these conversion values, a direct correlation was observed between higher HDS activity and decreasing crystal size as estimated from the Scherrer equation. These results suggest that such composites represent interesting and promising precursors for HDS catalysts, where the activity and stability can be modified either by chemical or structural changes of the composites under different conditions.

Received 9th June 2012,
Accepted 26th November 2012

DOI: 10.1039/c2dt31248d

www.rsc.org/dalton

1. Introduction

One of the most recent advances in materials science in the last decade concerns the harmonization and cooperative assembly of different material families into a single material, in order to access novel composites with improved or unusual exciting properties as a consequence of synergistic effects between both components.[1–5] In particular, the controllable preparation of novel hierarchical hybrid nano/microstructured composites continues to be a great challenge for researchers in materials science. Additionally, the integration of particles with different sizes (nano or micro) provides novel opportunities for studying structure–property relationships due to the possibility of fine tuning intrinsic physicochemical properties of each material that depend on their size (quantum size effect, surface resonance plasmon and tunnelling effect, *etc.*) and on their specific attachment or interface.[6–9] In this context, the hydrothermal method represents a powerful tool for the *one pot* synthesis of a

[a]*Centro de Química, Instituto Venezolano de Investigaciones Científicas, Apartado 20632, Caracas 1020-A, Venezuela*
[b]*Departamento de Ingeniería de Materiales y Nanotecnología, Instituto Venezolano de Investigaciones Científicas, Caracas, Venezuela*
[c]*PDVSA – Intevep, Los Teques 1070-A, Venezuela*
[d]*Unidad de Caracterización y Estructura de Materiales, Instituto Zuliano de Investigaciones Tecnológicas, Maracaibo, Venezuela*
[e]*Université Montpellier 2, Département Colloïdes, Verres et Nanomatériaux, Montpellier, France. E-mail: abriceno@ivic.gob.ve*

†Electronic supplementary information (ESI) available: FT-IR spectra, EDS analysis, XRPD patterns and TGA-air and N_2 analysis of the composites from hydrothermal synthesis of glucose and PMA; TEM images of MoO_3-phase from calcinations in air; XRPD pattern of the composite from glucose and PMA calcined in air for 5 minutes; FT-IR spectrum of the composite from hydrothermal synthesis of glucose and AHM; XRPD and SEM image of the nitride from MoO_2/C–N_2 composite; XRPD pattern, SEM images and EDS analysis of the sulfiding MoO_2/C composite; XRPD patterns and elemental analysis of catalysts after HDS reactions. See DOI: 10.1039/c2dt31248d

variety of core–shell materials with distinctive nano/microarray hybrid metal or metal oxide/carbon composites from direct carbonization of biomass or carbohydrates in the presence of metal species using mild conditions.[10–16] This method represents an interesting strategy for the preparation of heterostructures *via* a *bottom-up* approach[17,18] through the *in situ* formation of a carbonaceous material from molecular precursors and the incorporation of metal species either onto its surface (core–shell like) or by encapsulation (egg-yolk like).[19–24]

On the other hand, important efforts have been made in order to improve and find more active and stable heterogeneous catalysts. In particular, the doping or the addition of carbon, nitrogen, and phosphorous for the synthesis of transition metal carbides, nitrides and phosphides has attracted much attention due to their noble metal-like catalytic properties.[25–27] Thus, Mo and W carbides and nitrides represent interesting alternatives for their use in hydrotreatment reactions.[28–31] Likewise, recent evidences support growing interest in the use of novel distinctive carbonaceous matrixes such as fullerenes, carbon nanotubes, nanosheets and nanofibers and nanoporous carbons as alternative supports of catalysts, which offer comparative advantages with regard to oxidic supports, *i.e.* γ-Al_2O_3. Thus, *e.g.*, carbon materials interact less with the precursor oxidic phases, allowing a more complete formation of the active sulfides when employing conventional active phases.[32–36] Therefore, the synthesis of hybrid metal oxide/carbon materials bearing supported metal oxide nanoparticles highly dispersed on the carbonaceous support remains an interesting route for the preparation of novel catalysts[37–40] with a superior performance in hydroprocessing, particularly in deep hydrodesulphurisation.

As part of ongoing efforts in the design and preparation of novel hybrid materials based on polyoxometalates (POM),[41–51] we have envisaged the chemical coupling of nanometric POM precursors with carbon materials as an attractive alternative to design and generate hybrid materials through the concomitant *in situ* formation of colloidal carbon spheres from carbohydrates and the incorporation of POM onto their surface. Herein, we have explored such possibility in order to prepare novel nano/microcomposites as potential catalysts and/or catalytic precursors for the hydrodesulphurization reaction (HDS). Furthermore, we evaluated different synthetic parameters (reaction time, POM/glucose ratio and POM precursor) in order to study their effect on the synthesis of carbon microspheres decorated with molybdenum oxide nanoparticles from hydrothermal carbonization of glucose as a carbon precursor and phosphomolybdic acid (PMA) as a POM precursor. Likewise, to study the influence of another Mo-based POM on the morphology and microstructure of the carbonaceous material, ammonium heptamolybdate tetrahydrate (AHM) was also evaluated. Subsequent transformations in the solid state through calcinations of composites, nanostructured molybdenum dioxide or trioxide, were obtained. In addition, the composites were further transformed into carbon-supported Mo carbide or nitride. All these samples were *in situ* presulphided and tested in the HDS of thiophene at 400 °C and atmospheric pressure.

2. Experimental section

2.1. Hydrothermal synthesis of Mo–carbon composites

Anhydrous α-D-glucose, phosphomolybdic acid [$H_3PMo_{12}O_{40}$] (PMA) and ammonium heptamolybdate tetrahydrate [$(NH_4)_6Mo_7O_{24}$]·$4H_2O$ (AHM) were obtained from Aldrich Co. The reaction was carried out in a 23 mL capacity Teflon-lined stainless steel autoclave, which was introduced into a programmable oven. In a typical experiment, 1 g of glucose was dissolved in 10 mL of distilled water and the metal precursor was added to the glucose solution. The carbohydrate : metal salt molar ratio was varied from 40.5 : 1 to 13.5 : 1. The autoclave was sealed and heated at 180 °C for a chosen time between 6, 12 and 24 h and then allowed to cool to room temperature. The solid products were filtered off, washed several times with distilled water, and finally dried in a vacuum oven at 60 °C for 4 h.

2.2. Chemical and structural transformations of MoO_2/C composites

After hydrothermal synthesis, the transformations in the solid state of the metal oxide/carbon composites were achieved using several treatments. (1) Calcination in air, heating at 10 °C min^{-1} up to 500 °C and holding at this temperature for 4 h or 5 min, leading to either hollow metal oxide microspheres or MoO_2/C with cauliflower-like morphology, respectively. (2) Calcination under a 50 mL min^{-1} nitrogen flow at 10 °C min^{-1}, up to 500 °C and holding for 1 h, leading to recrystallized MoO_2/C–N_2 composites. (3) Carbiding under 50 mL min^{-1} of a CH_4 (20 vol%)–H_2 flow, heating at 5 °C min^{-1}, up to 600–800 °C and keeping the highest temperature for 2 h, leading to Mo_2C/C composites. (4) Nitriding under 50 mL min^{-1} of an NH_3 flow, heating at 5 °C min^{-1}, up to 700 °C and holding for 2 h, leading to MoN/C composites. After carbiding or nitriding treatments, the samples were quenched to room temperature and then passivated with an O_2 (1 mol%)–Ar mixture (see Scheme 1).

2.3. Preliminary study of thiophene hydrodesulphurization (HDS)

Before the HDS reaction, samples (200 mg) were submitted to a sulfiding pretreatment, which was carried out under a 1 vol% CS_2–H_2 mixture at 300 °C for 2 h. Tests of thiophene (C_4H_4S) HDS were performed in a continuous flow reactor with a fixed bed at 400 °C and atmospheric pressure. Test conditions were: 200 mg of catalyst, flow of 100 mL min^{-1} of a thiophene (2.27 mol%)–H_2 mixture. Reaction products were analyzed by means of gas chromatography with FID detection, with sampling of the gaseous effluent occurring at 15 min intervals until a stationary state was reached.

2.4. Characterization

The products were characterized by X-ray powder diffraction (XRPD) in reflection mode using Cu Kα radiation with a D8 FOCUS-BRUKER diffractometer, FT-IR spectroscopy with a Thermo Scientific Nicolet iS10, thermo-gravimetric analysis

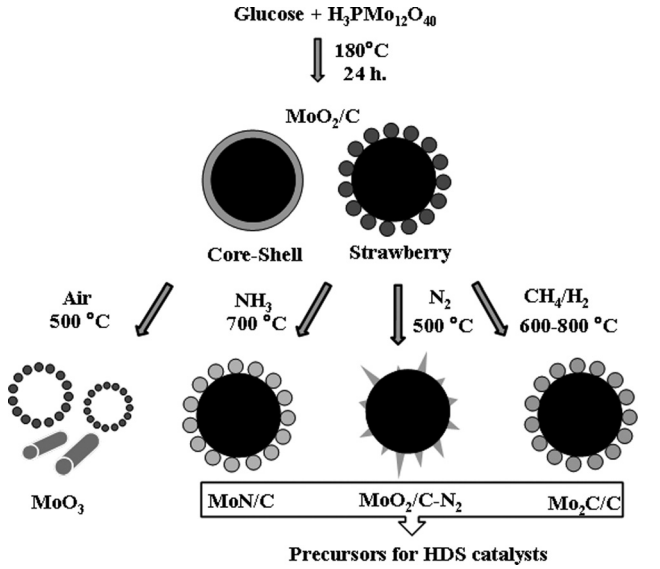

Scheme 1

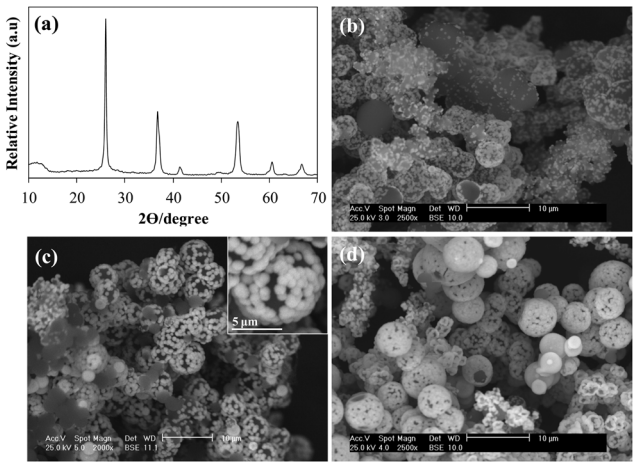

Fig. 1 (a) XRPD pattern of composite from a hydrothermal synthesis of glucose and PMA with a molar ratio of 20 : 1. SEM images of composites obtained from a hydrothermal synthesis of glucose and PMA with different ratios: (b) 40.5 : 1, (c) 20 : 1 and (d) 13.5 : 1.

(TGA) with a METTLER TOLEDO TGA/DSC1 STAR^e System and elemental analysis with a FISONS EA 1108 CHNS-0. The particle size and morphology were analyzed using a PHILLIPS XL30 scanning electron microscope (SEM) and a JEOL 1220 transmission electron microscope (TEM) operating at 200 keV. Nitrogen adsorption/desorption isotherms were measured at 77 K with a Micromeritics ASAP 2010. For the determination of the surface area, the BET method was employed.

3. Results and discussion

3.1. Synthesis and characterization of hierarchical MoO_2/C composites

The optimization of the hydrothermal carbonization conditions was first carried out for glucose, and afterwards for glucose in the presence of POM. In the case of carbonization of glucose and PMA, by varying the glucose : PMA molar ratios as 40.5 : 1, 20 : 1 and 13.5 : 1, an appreciable yield of carbonaceous material, regarding the starting materials, of 30, 41 and 50%, respectively, was achieved.

FT-IR spectra (see ESI, Fig. S1†) of the materials obtained from the hydrothermal synthesis of glucose and PMA with molar ratios of 40.5 : 1, 20 : 1 and 13.5 : 1 reveal that higher concentrations of PMA result in an increment of the intensity of the band at 964 cm^{-1}, which is attributed to the Mo═O groups. In contrast, the intensity of the peak corresponding to the C═O groups (1694 cm^{-1}) and the bandwidth of the O–H groups (3000–3500 cm^{-1}) both decrease, due to the interaction between these functional groups and metal species. X-ray powder diffraction (XRPD) was used to identify inorganic phases. Fig. 1(a) presents the XRPD pattern of the sample with a glucose : PMA molar ratio of 20 : 1, which reveals the presence of a highly crystalline phase, as well as background radiation due to the contribution of amorphous carbon spheres. All the diffraction peaks can be assigned to the pure monoclinic MoO_2 phase with lattice parameters a = 5.607 Å, b = 4.06 Å and c = 5.537 Å, β = 119.37°, which are in good agreement with the literature values (ICSD 00-032-0671). No additional diffraction peaks are found, confirming that the composite material corresponds to MoO_2 supported on carbon microspheres. By using Scherrer's equation, the average size of the MoO_2 nanoparticles is estimated to be 62 nm from the (−111)-plane of highest intensity (2θ = 26.03°).

Fig. 1(b)–(d) show the backscattering electron (BSE) images of the hybrid materials obtained from a synthesis of glucose and PMA with molar ratios of 40.5 : 1, 20 : 1 and 13.5 : 1, respectively. The micrographs show small microspheres formed of nanoaggregates corresponding to MoO_2 decorating carbon spheres, showing a strawberry-like morphology in the products of molar ratios 20 : 1 and 13.5 : 1. Carbon cores exhibit diameters of around 1–5 μm, indicating that the obtained nano/microstructures are polydisperse. Besides, SEM images further reveal that by increasing the amount of PMA, more MoO_2 species are positioned on the carbon microspheres surface, leading to MoO_2/C core–shell composites. For glucose : PMA ratios of 40.5 : 1 and 20 : 1, some uncoated carbon microspheres were observed. These results indicate that the concentration of PMA influences the crystallization of metal species, where the higher concentration of PMA enhances their growth and sintering, leading to a more compact and uniform oxide shell. In addition, EDS analysis (Fig. S2†) indicates that the samples consist exclusively of Mo, C and O.

These results were reinforced by chemical elemental analysis, which shows a C and H content of around 31 and 2%, respectively, for the material obtained from a hydrothermal synthesis of glucose and PMA with a molar ratio of 20 : 1. The remaining mass can be attributed to the oxygen and the inorganic species on the shell. The synthesized hybrid material

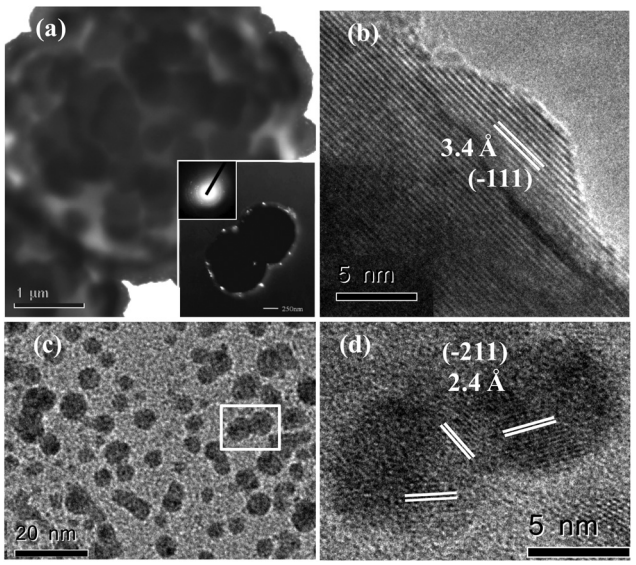

Fig. 2 (a) TEM image and SAED pattern (inset), and (b) HRTEM image of a MoO_2/carbon composite derived from a glucose : PMA ratio of 20 : 1. (c) and (d) HRTEM images of MoO_2 dispersed nanoparticles after ultrasonic treatment of the starting composite.

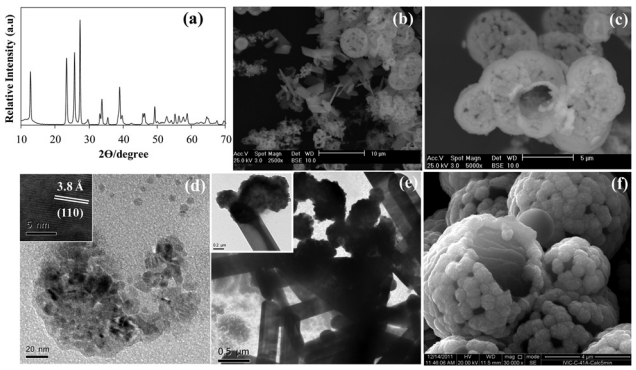

Fig. 3 (a) XRPD pattern of MoO_3 derived from a glucose : PMA ratio of 20 : 1, and calcined in air for 4 h. (b, c) SEM images and (d, e) TEM images of MoO_3. (f) SEM image of the composite calcined in air for 5 min.

was further investigated by means of transmission electron microscopy (TEM). Fig. 2 displays the images and the corresponding selected area electron diffraction (SAED) patterns of the MoO_2/C composite obtained from a hydrothermal synthesis of glucose and PMA (molar ratio 20 : 1). The TEM image in Fig. 2(a) confirms that MoO_2 spheres are effectively decorating the carbon surface.

According to the dark-field TEM image (inset), the shell is composed of aggregated nanoparticles with an approximate size of 25–75 nm. The estimated value by Scherrer's equation (62 nm) is included in this range. The selected area electron diffraction pattern shows a points and ring pattern, indicating that the shell of the carbon microspheres is made up of nanocrystals and polycrystalline aggregates, respectively. On the basis of the HRTEM images, arrangements of crystallographic planes can be appreciated. The planar space of lattice fringes is about 3.4 Å, corresponding to the (−111)-plane of MoO_2 (2θ = 26.03°). Additionally, these composites were subjected to ultrasonic treatment for 5 min, and the suspended solids were analyzed by HRTEM. The formation of dispersed MoO_2 nanoparticles, due to the detachment and fracture of the spherical MoO_2 nanoaggregates from the carbon spheres, was observed (Fig. 2(c)). These nanoparticles range from 5 to 15 nm in diameter. The HRTEM image displays arrangements of crystallographic planes, in which the (−211)-plane with an interplanar distance of 2.4 Å was identified (2θ = 37.03°).

On the other hand, when the carbonization of the glucose : PMA molar ratio of 20 : 1 was carried out varying the reaction time (6 and 12 h), a decrease of the yield of carbonaceous materials of 15 and 22% was observed, regarding the material obtained at 24 h. The carbonization at different times leads to remarkable changes in XRPD patterns (Fig. S3†). At 6 h, the XRPD pattern reveals that the resulting phase is amorphous. However, by increasing the time (12 h), some signals of low intensity corresponding to MoO_2 (37, 41 and 53°) can be appreciated and the sample becomes more crystalline. Therefore, these results indicate that reaction time plays an important role in the formation of the MoO_2 phase, where effectively 24 h is the appropriate time for improving the crystallinity.

3.2. Transformations of the composites in the solid state upon calcinations in air and N_2

Additionally, we characterized the solid obtained from the glucose : PMA ratio of 20 : 1 through thermo-gravimetric analysis (TGA) in air and nitrogen (Fig. S4†). The TG curve using air exhibited the main weight loss between 250 and 500 °C attributed to the elimination of the carbon core. From 500 to 800 °C, no other weight loss was detected. The TG curve using nitrogen exhibited a gradual and not pronounced weight loss between 250 and 800 °C, attributed to the partial elimination of organic volatiles from the carbonaceous matrix. On the basis of both analyses, we anticipate that the controlled calcination of the composite upon different conditions should lead to interesting transformations in the solid state in order to obtain novel molybdenum oxide nano/microcomposites.

Thereby, the composite derived from the glucose : PMA ratio of 20 : 1 was calcined in static air at 500 °C (heating rate of 10 °C min^{-1}) for 4 h to remove the carbon core. Fig. 3(a) presents the XRPD pattern, which reveals a high crystallinity of the resulting metal oxide. In comparison to the starting composite, no background radiation is shown due to the remotion of amorphous carbon. All the diffraction peaks can be easily assigned to the pure orthorhombic phase of α-MoO_3 with lattice parameters a = 3.962 Å, b = 13.858 Å and c = 3.697 Å, which are in good agreement with the literature values (ICSD 00-005-0508). No other diffraction peaks were found. By using Scherrer's equation, the average size of the MoO_3 nanoparticles is estimated to be 79 nm from to the (021)-plane of highest intensity (2θ = 27.28°).

As expected, SEM images (Fig. 3(b, c)) show that after the calcination treatment in air, the sample forms metal oxide hollow microspheres together with microrod and plate-like

characteristics of the MoO_3 phase. Interestingly, two broken spheres can be observed by SEM and TEM (Fig. 3(d, e)), showing that effectively the spheres are hollow, with similar diameters as those of the starting composite, in the range of 500 nm to 5 μm with a dense wall thickness. These hollow spheres are made up of aggregates of nanoplates with sizes of 50–80 nm. The value estimated by Scherrer's equation (79 nm) is included in this range. Additionally, smaller spherical nanoparticles were observed, which range from 5 to 10 nm (Fig. S5†). EDS analysis (not shown) indicates that the sample consists only of Mo and O. Likewise, elemental analysis demonstrates the absence of C and H.

In Fig. 3(d) (inset), arrangements of crystallographic planes can be appreciated. The interplanar spacing of lattice fringes is about 3.8 Å, corresponding to the (110)-plane of the MoO_3 phase ($2\theta = 23.33°$). These results demonstrate that upon calcinations in air, topotactic transformations in the solid state take place from MoO_2 to MoO_3 and constitute an attractive alternative to obtain nanostructured hollow spheres.

Fig. 3(e) depicts different types of morphologies: aside from the usual expected hollow spheres, a large number of rod-like structures were also observed. These rods have diameters from 250 to 750 nm, approximately. Noteworthy, Fig. 3(e) (TEM inset) shows spheroidal structures located on the top of a nanorod, suggesting the incipient crystallization of MoO_3 from the starting microspheres. Nevertheless, when the composite was calcined in air for 5 minutes at 500 °C, neither nanorod nor microcrystal formations were observed by SEM analysis, but composites with a cauliflower-like morphology bearing a remaining carbon core were observed (Fig. 3(f)). The elemental analysis shows a decrease of C content of around 20%. Surprisingly, the XRPD pattern shows the absence of MoO_3 and the preservation of MoO_2/C (Fig. S6†), which could be accounted for by the strong reducing nature of the carbon core. This observation reveals that the calcination treatment time influences the crystallization and/or sinterization process of hollow MoO_3 microspheres.

Furthermore, the hybrid material derived from the glucose : PMA ratio of 20 : 1 was heated at 10 °C min^{-1} up to 500 °C under nitrogen atmosphere and held for 1 h at this temperature (MoO_2/C–N_2). The XRPD pattern is similar to that of the initial monoclinic phase of MoO_2, which is thus preserved during the thermal treatment (Fig. 4(a)). By using Scherrer's equation, the average size of the MoO_2 nanoparticles is estimated to be 19 nm from to the (−111)-plane of highest intensity ($2\theta = 26.08°$). Interestingly, SEM and TEM images reveal a remarkable morphology evolution from MoO_2 spherical nanoaggregates to nanoneedles decorating carbon spheres, showing an urchin-like topology (Fig. 4(b)). In fact, the MoO_2 phase was preserved in spite of changing its morphology, which is attributed to partial recrystallization during the calcination process under nitrogen atmosphere. In addition, EDS analysis (not shown) indicates that the samples contain Mo, C, O. These results were reinforced by elemental analysis (%C and H content around 18 and 1%, respectively), which reveals the presence of a remaining carbon core.

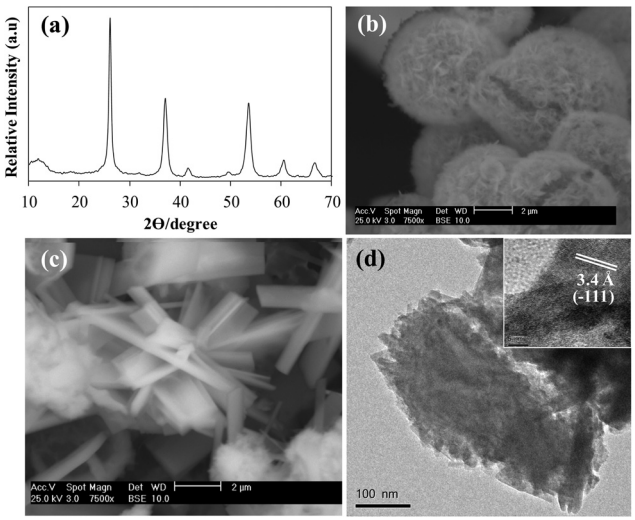

Fig. 4 (a) XRPD pattern, (b, c) SEM images and (d) TEM image of MoO_2/C–N_2.

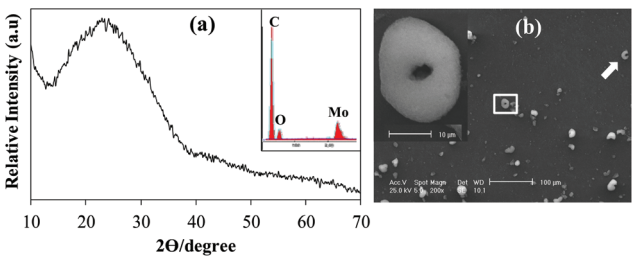

Fig. 5 (a) XRPD pattern, EDS analysis (inset) and (b) the SEM image of the hybrid material obtained from a hydrothermal synthesis of glucose and AHM.

3.3. Synthesis of Mo-composites using another POM precursor

In order to study the effect of another molybdenum-based POM on the morphology and microstructure of the carbonaceous material, ammonium heptamolybdate tetrahydrate $[(NH_4)_6Mo_7O_{24}]\cdot 4H_2O$ (AHM) was also used. Thereby, hydrothermal carbonization of glucose in the presence of AMH (glucose : AHM molar ratio 20 : 1, at 180 °C for 24 h) was carried out, in which an appreciable yield of 55% was obtained. In the FT-IR spectrum (Fig. S7†) the bands corresponding to Mo═O (900–950 cm^{-1}), C═O (1690 cm^{-1}) and O–H (3000–3500 cm^{-1}) groups can be appreciated. The XRPD pattern (Fig. 5(a)) indicates that the resulting phase is amorphous. Noteworthy, the SEM image (Fig. 5(b)) reveals remarkable changes in the morphology, when HMA was used. The carbonaceous material consists of irregular aggregates in combination with ring-like microstructures of 20 μm in diameter, approximately. Interestingly, broken microrings can be observed (shown by the arrow). Besides, EDS analysis confirms that the sample is made up of Mo, C and O.

While our work was in progress, a similar MoO_2–carbon composite was independently synthesized by Duo and Zeng by using another Mo-precursor (Na_2MoO_4) and slightly different experimental conditions.[45] However, the authors reported that

MoO_2 nanoparticles were found embedded into carbon microspheres (MoO_2@C) in contrast to our results, where MoO_2 is located decorating the carbon surface (MoO_2/C). On the basis of these results, we can observe that POMs play an important role on the structural characteristics of the products. Additional studies have evaluated the effect of POMs on the morphology of carbonaceous materials under hydrothermal conditions. Due to their electronic properties and structural robustness, POMs (*i.e.*, phosphomolybdic acid, tungstosilicic acid, tungstophosphoric acid, phosphovanadomolybdate and ammonium metavanadate) have been exploited as promising catalysts, promoters and/or oxidizing agents in order to modify the structure of carbohydrates-derived carbon and active carbon, leading to carbon nanotubes, nanobelts, nanoparticles, nanospheres or core–shell composites.[46–49] Therefore, we believe that the changes in the morphology of carbonaceous materials could be mainly attributed to the difference in the reduction potential of PMA and AHM, which involves distinct oxidation–reduction reactions between aldehyde-like intermediates (reducing agent) from glucose-derived dehydration products or intermediates[52,53] and POMs (oxidizing agent). In the case of metal oxide/carbon composites, PMA (Mo^{6+}) is reduced to MoO_2 (Mo^{4+}), where the carboxylate or carboxylic groups on the surface of carbon spheres can interact with MoO_2, resulting in the formation of the different composites.

3.4. Synthesis of carbides and nitrides from MoO_2/C composites

Taking advantage of our ongoing studies about the synthesis and characterization of metal carbides and nitrides as interesting catalytic precursors for a hydrodesulphurization (HDS) reaction,[28–31] we explored the possibility of generating Mo carbides and nitrides by chemical transformations in the solid state from MoO_2/C as a precursor (glucose : PMA molar ratio 20 : 1).

Fig. 6 shows the XRPD patterns of the materials obtained from nitriding (at 700 °C) and carbiding (at 600, 700 and 800 °C) treatments of MoO_2/C composites. For the product of the nitriding treatment, the diffraction peaks can be assigned to the MoN phase with lattice parameters a = 5.725 Å, c = 5.608 Å and γ = 120°, which are in good agreement with the literature values (ICSD 00-025-1367). The carbiding at different temperatures leads to remarkable changes in the XRD signals, indicating that by increasing the temperature the inorganic phase becomes even more crystalline. At 800 °C, the peaks can be identified as the phase of Mo_2C with lattice parameters a = 3.012 Å, c = 4.735 Å and γ = 120°, in good agreement with the literature values (ICSD 00-035-0787). By using Scherrer's equation, the average size of both MoN and Mo_2C nanoparticles is estimated to be 9 nm from to the (200)-plane (2θ = 36.17°) and (101)-plane (2θ = 39.38°) of highest intensity, respectively.

Fig. 7 displays SEM images of the material obtained from nitriding (at 700 °C) and carbiding (at 600 and 800 °C) treatments of MoO_2/C composites. In such images, either individual or sinterized nanoaggregates corresponding to MoN or

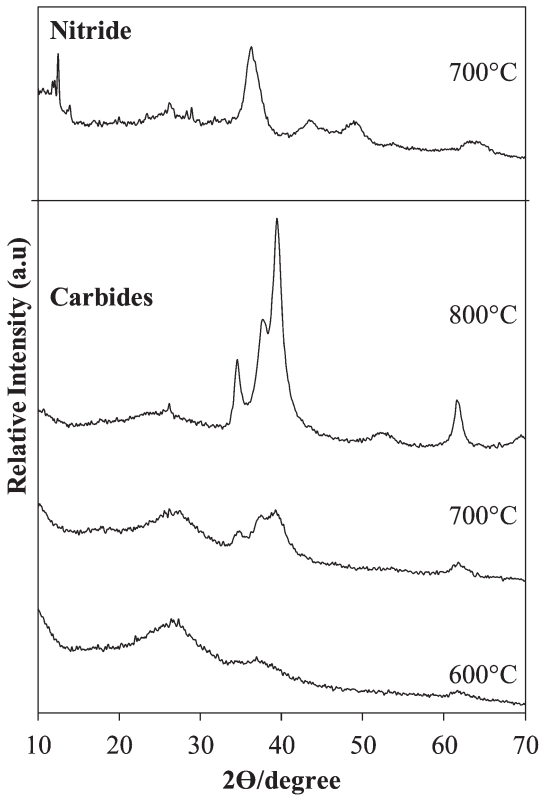

Fig. 6 XRPD patterns of the material obtained from nitriding (at 700 °C) and carbiding (at 600, 700 and 800 °C) treatments of MoO_2/C strawberry-like composites.

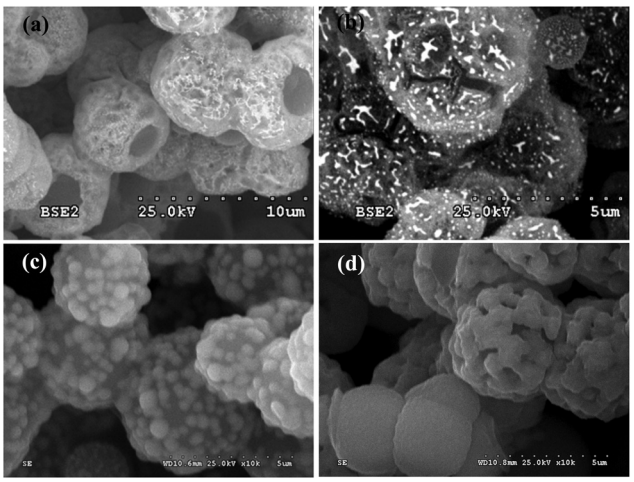

Fig. 7 SEM images of MoN/C obtained by nitriding at 700 °C (a, b) and Mo_2C/C by carbiding at 600 (c) and 800 °C (d), respectively.

Mo_2C can be distinguished, which are found decorating strawberry-like spherical carbon cores or the formation of porous MoN/C or Mo_2C/C core–shell composites. In particular, an increase of temperature from 600 to 800 °C during the carbiding process leads to the sinterization of the aggregates on the surface (Fig. 7(c, d)). As was observed for the starting composites, the core/shell structures are polydisperse, exhibiting a

mean diameter of around 5 μm. Notably, the morphology of the carbon cores were preserved after treatment, thus representing effective hard templates in the synthesis of either Mo nitrides or carbides. Likewise, inorganic nanoaggregates positioned on the shell were preserved, in spite of the crystalline phase change. These results suggest that such transformations occur *via* topotactic transformations in the solid state from MoO_2/C to MoN/C or Mo_2C/C nano/microcomposites, respectively.

In addition, elemental analysis of MoN/C shows a C, N and H content of around 24, 5 and 2%, respectively. The remaining mass can be attributed to the oxygen and the molybdenum in the shell. This result confirms that effectively the inorganic phase corresponds to MoN, as the nitrogen (5%) and molybdenum (30%) contents are equivalent to a Mo : N molar ratio of 1 : 1. In the case of Mo_2C/C, a carbon content around 40% (remaining mass of oxygen and molybdenum) without the presence of hydrogen or nitrogen was obtained.

3.5. Study of the catalytic activity of the materials on thiophene hydrodesulfurization (HDS)

Finally, a preliminary study on thiophene hydrodesulfurization using the synthesized hybrid materials was carried out. Fig. 8 shows the thiophene HDS conversion as a time-function for various presulphided samples. As can be appreciated, MoN/C exhibits the highest initial conversion (77.9%), followed by Mo_2C/C (60.0%). These two materials lead to higher initial conversion than the MoO_2/C starting composite (39.2%). Generally, transition metal carbides and nitrides have been shown to possess better HDS activity than the corresponding oxides or sulfides.[28,54,55] The textural properties of these materials could also play a role, as the initial activity trend parallels that of the surface areas of these three samples (Table 1). On the other hand, we evaluated the HDS conversion using urchin-like composites (MoO_2/C–N_2). Notably, a different behavior in the thiophene HDS curve between MoO_2/C–N_2 and its MoO_2/C mother-phase was observed. Initially, conversion of MoO_2/C is greater than MoO_2/C–N_2. However, from 45 min the conversion of the latter is higher and shows more stability than that of MoO_2/C. The higher initial activity can be attributed to the higher surface area of MoO_2/C than that of MoO_2/C–N_2. On the basis of these results, we compared thiophene HDS between the catalysts with the best initial conversion (MoN/C) and the material obtained by nitriding MoO_2/C–N_2 urchin-like composites (MoN/C–N_2). Previously, this material was analyzed by the XPRD pattern, confirming the formation of the MoN phase. Besides, SEM images show a core/shell morphology, which was likely formed from sinterization of MoO_2 nanoneedles during the nitriding treatment (Fig. S8†). As shown in Table 1, MoN/C–N_2 exhibits an initial conversion of 51%, which is lower than that of MoN/C. However, the steady state conversion is comparable for these two materials. Noteworthy, from 45 min the conversion behavior of the latter is slightly more stable than that of MoN/C. Therefore, the different long term stabilities suggest that morphology (spheres, needles, core–shell and plates) plays an important role in the HDS conversion and stability of the catalysts.

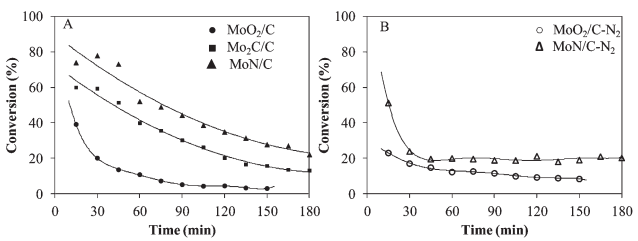

Fig. 8 Thiophene hydrodesulfurization conversion (%) as a function of time (min) using (A) MoO_2/C, MoN/C and Mo_2C/C; (B) MoN/C–N_2 and MoO_2/C–N_2.

Several studies have stressed the effect of morphology on the catalytic activity, adsorption processes and sensor sensibility.[56–60] Taking into account all the steady-state conversion values, a direct correlation between higher HDS activity and decreasing crystal size was observed (Table 1). Conversely, no correlation exists between surface area and either initial or steady-state activities. A summary of morphology, activity, texture and crystallite size of all the catalysts studied is shown in Table 1.

After the sulfiding pretreatment of the MoO_2/C mother-phase, the XRPD pattern shows the preservation of the MoO_2 bulk phase (Fig. S9†). The SEM image reveals a partial morphology change of the strawberry-like MoO_2/C to core–shell composites with the presence of small hollows on the shell. Besides, some hollow and broken spheres can be observed, which can be attributed to a partial oxidation of carbon cores during the sulfiding treatment. Likewise, further analyses by XRPD of all the catalysts used after the HDS reaction reveal the preservation of the initial bulk phases (Fig. S10†). Elemental analysis shows the partial sulfiding of all the phases with S content percentages between 3 and 7% (Table S1†). These results suggest surface sulfiding of the nanostructured catalysts, in agreement with the known stability either of this

Table 1 Initial conversion, steady-state conversion, surface area and estimated crystallite size by Scherrer's equation of the catalysts in HDS reactions

Catalysts	Morphology	Initial conversion (%)	Steady-state conversion (%)	Surface area ($m^2\ g^{-1}$)	Estimated crystal size by Scherrer's equation (nm)
MoN/C–N_2	Core–shell	51	20	87	8
MoN/C	Strawberry	78	17	27	9
Mo_2C/C	Strawberry	60	15	16	9
MoO_2/C–N_2	Urchin	23	9	50	19
MoO_2/C	Strawberry	39	4	10	62

oxidic phase or of the carbides and nitrides. Besides, the results also support the claim that the active phases in the carbide/nitride catalysts are mixed combinations of MoO(S)/C, MoN(S)/C and Mo_2C(S)/C phases.[29–31,53,54]

4. Conclusions

In summary, we have described a simple *bottom-up* route for the synthesis of novel MoO_2/C nano/microcomposites from the hydrothermal carbonization of a solution of glucose as a carbon precursor in the presence of polyoxometalates such as phosphomolybdic acid or ammonium heptamolybdate tetrahydrate. This *one-pot* method allows the synthesis of a variety of controllable metal oxide/carbon composites with distinctive nano/microdomain arrays. Likewise, these composites can be transformed into complex nanostructured materials (hollow spheres, core–shell, strawberries, cauliflowers, rods, urchins, plates and nanoparticles) including molybdenum oxides, nitrides or carbides supported onto carbon microspheres. These hybrid materials represent interesting and promising precursors for HDS catalysts, where the activity and stability could be fine-tuned from the chemical and morphological modification of the composites under different conditions. Further studies for improving the performance of such catalysts by the addition of different amounts of metallic promoters (Co and Ni) are in progress.

Acknowledgements

This work was supported in part by FONACIT through grants G-2005000433 and G-2000001537. We thank Miguel Angel Ramos (INZIT); Lisbeth Lozada, Antonio Monsalve, Yraida Díaz, Eleinne Severino (IVIC); and Anthony Bilot (Université Montpellier 2) for technical assistance. C.A. is grateful to FONACIT and to Sylvie Calas, Florence Despetis and Rémi Courson for training during a visiting fellowship to Université Montpellier 2, through the PCP program Venezuela-France, "Materiales nanoestructurados para el desarrollo sostenible".

References

1 G. Férey, *Dalton Trans.*, 2009, 4400.
2 M. F. Ashby and Y. J. M. Bréchet, *Acta Mater.*, 2003, **51**, 5801.
3 S. Chandra, K. C. Barick and D. Bahadur, *Adv. Drug Delivery Rev.*, 2011, **63**, 1267.
4 B. Zambrano, E. Cañizalez, P. Silva and A. Briceño, *New J. Chem.*, 2011, **35**, 288.
5 A. Bordoloi, N. T. Mathew, F. Lefebvre and S. B. Halligudi, *Microporous Mesoporous Mater.*, 2008, **115**, 345.
6 S. Guo and E. Wang, *Acc. Chem. Res.*, 2011, **44**, 491.
7 A. Moores and F. Goettmann, *New J. Chem.*, 2006, **30**, 1121.
8 J. W. Steed, D. R. Turner and K. J. Wallace, *Core Concepts in Supramolecular Chemistry and Nanochemistry*, Wiley, England, 2007.
9 C. Joachim, *Nat. Mater.*, 2005, **4**, 107.
10 B. Hu, K. Wang, L. Wu, S.-H. Yu, M. Antonietti and M.-M. Titirici, *Adv. Mater.*, 2010, **22**, 813.
11 B. Hu, S.-H. Yu, K. Wang, L. Liu and X.-W. Xu, *Dalton Trans.*, 2008, 5414.
12 K. Byrappa and T. Adschiri, *Prog. Cryst. Growth Charact. Mater.*, 2007, **53**, 117.
13 M.-M. Titirici, M. Antonietti and A. Thomas, *Chem. Mater.*, 2006, **18**, 3808.
14 Y. Meng, D. Chen and X. Jiao, *Eur. J. Inorg. Chem.*, 2008, 4019.
15 C.-Y. Lee, S.-J. Kim, I.-S. Hwang and J.-H. Lee, *Sens. Actuators, B*, 2009, **142**, 236.
16 M.-M. Titirici, A. Thomas and M. Antonietti, *Adv. Funct. Mater.*, 2007, **17**, 1010.
17 T. N. Hoheisel, S. Schrettl, R. Szilluweit and H. Frauenrath, *Angew. Chem., Int. Ed.*, 2010, **49**, 2.
18 S. Venkataraman, J. L. Hedrick, Z. Y. Ong, C. Yang, P. L. R. Ee, P. T. Hammond and Y. Y. Yang, *Adv. Drug Delivery Rev.*, 2011, **63**, 1228.
19 G. Yu, B. Sun, Y. Pei, S. Xie, S. Yan, M. Qiao, K. Fan, X. Zhang and B. Zong, *J. Am. Chem. Soc.*, 2010, **132**, 935.
20 J. C. Park and H. Song, *Chem. Mater.*, 2007, **19**, 2706.
21 J. Yu, X. Yu, B. Huang, X. Zhang and Y. Dai, *Cryst. Growth Des.*, 2009, **9**, 1474.
22 X. Sun and Y. Li, *Angew. Chem., Int. Ed.*, 2004, **43**, 597.
23 B. Zhang, X. Yu, C. Ge, X. Dong, Y. Fang, Z. Li and H. Wang, *Chem. Commun.*, 2010, **46**, 9188.
24 H. Wang, Y.-B. Sun, Q.-W. Chen, Y.-F. Yu and K. Cheng, *Dalton Trans.*, 2010, **39**, 9565.
25 E. Antolini and E. R. González, *Appl. Catal., B*, 2010, **96**, 245.
26 R. Wang, C. Tian, L. Wang, B. Wang, H. Zhang and H. Fu, *Chem. Commun.*, 2009, 3104.
27 A.-M. Alexander and J. S. J. Hargreaves, *Chem. Soc. Rev.*, 2010, **39**, 4388.
28 P. Rodríguez, J. L. Brito, A. Albornoz, M. Labady, C. Pfaff, S. Marrero, D. Moronta and P. Betancourt, *Catal. Commun.*, 2004, **5**, 79.
29 E. Puello-Polo, A. Gutiérrez-Alejandre, G. González and J. L. Brito, *Catal. Lett.*, 2010, **135**, 212.
30 E. Puello-Polo and J. L. Brito, *J. Mol. Catal. A: Chem.*, 2008, **281**, 85.
31 E. Puello-Polo and J. L. Brito, *Catal. Today*, 2010, **149**, 316.
32 E. Furimsky, *Carbon and Carbon Supported Catalysts in Hydroproccesing*, ed. J. J. Spivey, RSC Catalysis Series, Ottawa, Ontario, Canada, 2007, vol. 16–18, p. 1.
33 P. A. Nikulshin, N. N. Tomina, A. A. Pimerzin, A. V. Kucherov and V. M. Kogan, *Catal. Today*, 2010, **149**, 82.
34 F. Liu, S. Xu, Y. Chi and D. Xue, *Catal. Commun.*, 2011, **12**, 521.

35 H. Shang, C. Liu, Y. Xu, J. Qiu and F. Wei, *Fuel Process. Technol.*, 2007, **88**, 117.
36 A. N. Pour, A. M. Rashidi, K. J. Jozani, A. Mohajeri and P. Khorami, *J. Nat. Gas Chem.*, 2010, **19**, 91.
37 P. Makowski, R. Demir Cakan, M. Antonietti, F. Goettmann and M.-M. Titirici, *Chem. Commun.*, 2008, 999.
38 R. Demir-Cakan, P. Makowski, M. Antonietti, F. Goettmann and M.-M. Titirici, *Catal. Today*, 2010, **150**, 115.
39 J. Matos, M. Rosales, R. Demir-Cakan and M. M. Titirici, *Appl. Catal., A*, 2010, **386**, 140.
40 J. Matos, A. García, L. Zhao and M. M. Titirici, *Appl. Catal., A*, 2010, **390**, 175.
41 A. Briceño, A. Fulgence, Y. Hill and R. Atencio, *Dalton Trans.*, 2008, 3275.
42 R. Atencio, A. Briceño, P. Silva, J. A. Rodríguez and J. C. Hanson, *New J. Chem.*, 2007, **31**, 33.
43 R. Atencio, A. Briceño and X. Galindo, *Chem. Commun.*, 2005, 637.
44 Y. Wang and I. A. Weinstock, *Chem. Soc. Rev.*, 2012, **41**, 7479.
45 J. Dou and H. C. Zeng, *J. Phys. Chem. C*, 2012, **116**, 7767.
46 H. Fei, X. Ding, M. Wei and K. Wei, *Solid State Sci.*, 2011, **13**, 2049.
47 K. Pan, H. Ming, Y. Liu and Z. Kang, *New J. Chem.*, 2012, **36**, 113.
48 Z. Kang, E. Wang, B. Mao, Z. Su, L. Gao, S. Lian and L. Xu, *J. Am. Chem. Soc.*, 2005, **127**, 6534.
49 D.-L. Long, R. Tsunashima and L. Cronin, *Angew. Chem., Int. Ed.*, 2010, **49**, 1736.
50 D.-L. Long, E. Burkholder and L. Cronin, *Chem. Soc. Rev.*, 2007, **36**, 105.
51 A. Spojakina, E. Kraleva, K. Jiratova and L. Petrov, *Appl. Catal., A*, 2005, **288**, 10.
52 N. Baccile, G. Laurent, F. Babonneau, F. Fayon, M.-M. Titirici and M. Antonietti, *J. Phys. Chem. C*, 2009, **113**, 9644.
53 R. Demir-Cakan, N. Baccile, M. Antonietti and M.-M. Titirici, *Chem. Mater.*, 2009, **21**, 484.
54 J. W. Logan, J. L. Heiser, K. R. McCrea, B. D. Gates and M. E. Bussell, *Catal. Lett.*, 1998, **56**, 165.
55 B. Diaz, S. J. Sawhill, D. H. Bale, R. Main, D. C. Phillips, S. Korlann, R. Self and M. E. Bussell, *Catal. Today*, 2003, **86**, 191.
56 L. Zheng, Y. Xu, D. Jin and Y. Xie, *Chem. Mater.*, 2009, **21**, 5681.
57 R. Nava, B. Pawelec, J. Morales, R. A. Ortega and J. L. G. Fierro, *Microporous Mesoporous Mater.*, 2009, **118**, 189.
58 A. Tricoli, M. Righettoni and A. Teleki, *Angew. Chem., Int. Ed.*, 2010, **49**, 7632.
59 R. Huirache-Acuña, B. Pawelec, E. Rivera-Muñoz, R. Nava, J. Espino and J. L. G. Fierro, *Appl. Catal., B*, 2009, **92**, 168.
60 R. Habibi, A. M. Rashidi, J. T. Daryan and A. Mohamad ali zadeh, *Appl. Surf. Sci.*, 2010, **257**, 434.